Loop I/NPS morphology predictions in the ultralong-wavelength band

Yanping Cong, ¹ Bin Yue, ^{2,3} Yidong Xu, ^{2,3} Furen Deng, ^{2,4} Jiajun Zhang, ¹ and Xuelei Chen^{2,3,4}

¹Shanghai Astronomical Observatory, Chinese Academy of Sciences, Shanghai 200030, China

ABSTRACT

Loop I/North Polar Spur (NPS) is the giant arc structure above the Galactic plane observed in the radio sky. It is the most conspicuous feature in low frequency radio sky maps besides the galactic plane itself. There is a long-standing debate about its origin. While the majority consider it as a nearby supernova remnant (SNR), it has also been suggested to be a giant bubble close to the Galactic Center (GC), associated with the Fermi Bubble and eROSITA X-ray bubble. There is also the possibility that a nearby SNR and a bubble near the GC happens to overlay each other. At ultralong wavelength band (wavelength $\gtrsim 10$ m or frequency $\lesssim 30$ MHz), particularly below ~ 10 MHz, the free-free absorption of radio signal by the diffuse electrons in interstellar medium (ISM) becomes significant, resulting in sky morphology differs largely from higher frequencies. In this paper, we predict the Loop I/NPS morphology at ultralong wavelength band. We develop emissivity models for the two Loop I/NPS origin models. We find that, at ultralong wavelength band, for the SNR model, the full Loop I/NPS is still a bright arc even at frequency as low as ~ 1 MHz; however, in the GC model, the Loop I/NPS appears only at $b \gtrsim 30^{\circ}$, at $b \lesssim 30^{\circ}$ the Loop I/NPS is invisible due to the absorption by ISM electrons between the GC and the Sun. Upcoming ultralong wavelentgh projects such as DSL and FARSIDE can potentially distinguish these two models and provide decisive information about the origin of Loop I/NPS.

Keywords: Interstellar medium (847) — Interstellar plasma (851)— Interstellar absorption (831)— Milky Way Galaxy (1054) — Radio interferometers (1345)

1. INTRODUCTION

In the radio sky, Loop I exhibits a conspicuous giant loop-like (arc) feature above the Galactic plane (Baldwin 1955; Roger et al. 1999; Dowell et al. 2017; Eastwood et al. 2018; Guzmán et al. 2011; Landecker & Wielebinski 1970; Patra et al. 2015; Haslam et al. 1982; Reich & Reich 1986; Intema et al. 2017), covering an area of $\sim 70^{\circ} \times 50^{\circ}$ (Lallement 2023). It roots approximately at $l \sim 30^{\circ}$, $b \sim 10^{\circ}$, and extends to the north Galactic pole at about $l \sim 330^{\circ}$, $b \sim 80^{\circ}$. There is a brightest spur near Loop I's root (Hanbury Brown et al. 1960), named North Polar Spur (NPS, e.g. Iwashita et al. 2023). In this paper we use "Loop I/NPS" to refer to the full loop-like

Corresponding author: Bin Yue yuebin@nao.cas.cn

structure. In soft X-ray band, there is also a loop-like structure above Galactic plane, largely coincident with the radio Loop I/NPS (Egger & Aschenbach 1995). The X-ray structure is quasi-circular and is generally identified as a bubble, the Northern eROSITA bubble. Below the Galactic plane, there is also the Southern eROSITA bubble that is roughly symmetric to its sibling (Predehl et al. 2020). However, in radio band currently there is no coincident structure found in total intensity map.

Beside Loop I/NPS, other loop-like structures have also been found, and designated as Loop II (Cetus arc) (Large et al. 1962), Loop III (Quigley & Haslam 1965), and Loop IV (Large et al. 1966; Berkhuijsen et al. 1971). The Loop I structure, and many other smaller and dimmer loop-like structures, are highly polarized (Planck Collaboration et al. 2016). The polarized structure of

² National Astronomical Observatories, Chinese Academy of Sciences, 20A Datun Road, Chaoyang District, Beijing 100101, China
³ Key Laboratory of Radio Astronomy and Technology, Chinese Academy of Sciences, 20A Datun Road, Chaoyang District, Beijing 100101, China

⁴School of Astronomy and Space Science, University of Chinese Academy of Sciences, Beijing 100049, China

Loop I seems extend to far below the Galactic plane (Vidal et al. 2015; Panopoulou et al. 2021).

The debate on the origin of the Loop I/NPS structure, including the position and physical size, has persisted for over 40 years and remains contentious (e.g. Dickinson 2018; Planck Collaboration et al. 2016; Kataoka et al. 2018; Shchekinov 2018). Because of its huge angular size ($\sim 120^{\circ}$, Dickinson 2018), many people consider Loop I/NPS to be a nearby object within $\lesssim 1$ kpc, but the exact distance and geometry is still debated. One method for deriving the distance of Loop I/NPS is to analyze the alignment between optical starlight and the synchrotron polarization angles. These two angles should be significantly correlated with each other if the synchrotron radiation come from sources closer than stars, since the starlight polarization is generated by dust that traces magnetic field generating the synchrotron polarization. Moreover, the thermal dust emission polarization also traces the magnetic field. Panopoulou et al. (2021) analyzed the polarization angles of these three tracers, and derived upper limits on the Loop I/NPS distance, all are below ~ 150 pc. It strongly favors that the Loop I, at least the $b > 30^{\circ}$ part, is a near source. Some authors suggest that it is a superbubble neighboring the Local Hot Bubble (LHB) where we reside (Cox & Reynolds 1987), created by stellar winds and a series of supernova explosions happened in recent several million years in the Scorpius–Centaurus OB association that is ~ 170 pc away from the Sun (de Geus 1992; Breitschwerdt & de Avillez 2006). The Geminga pulsar is considered to be produced in such a supernova explosion (Burke et al. 2019). It is further pointed out that, the Loop I/NPS superbubble is interacting with the Local Hot Bubble (LHB) where we reside, and the interaction zone forms a dense HI ring (wall) between those two bubbles. The existence of the dense HI ring is supported by the sudden increase of HI column density at ~ 40 pc from Sun, indicated by the optical and UV absorption spectra of stars toward the center of Loop I/NPS (Centurion & Vladilo 1991); the coherence of X-ray absorption shadow and the HI column density distribution (Egger & Aschenbach 1995), and the strengthened intensity of far-UV O VI emission line (Sallmen et al. 2008).

However, the notion of a coherent ring structure formed by the interaction of Loop I/NPS with the LHB is questioned in some observations. For example, Reis & Corradi (2008) analyzed the color excess of more than 4000 stars up to 500 pc from Sun, and Santos et al. (2011) analyzed the optical polarization of more than 800 stars. They found that the interface between Loop I/NPS supperbubble and LHB is fragmented and distorted. Moreover, the analysis of X-ray absorption by

the gas between Loop I/NPS and the Sun indicates that Loop I/NPS could be more distant, about $\sim 500-1000$ pc away (Iwan 1980; Sofue 2015; Lallement et al. 2018). Faraday rotation depolarization and Faraday tomography methods also favor a distance of several hundred pc for Loop I/NPS, see reviews Dickinson (2018) and Lallement (2023), and references therein.

Some people instead propose that Loop I/NPS may originate from the Galactic Center (GC) (Sofue et al. 1974; Sofue 2000), based on its directional proximity and possible association with the eROSITA bubble at X-ray band, and the Fermi Bubble at gamma-ray band (Su et al. 2010; Predehl et al. 2020). Both the eROSITA bubble and Fermi bubble are split into two roughly symmetric parts by the Galactic plane, strongly favoring the GC hypothesis (Sofue 1977, 2000; Sofue et al. 2016). In such scenario, since the structure is located at $\sim 8 \text{ kpc}$ away, it must have considerable physical size (Sarkar 2019; Sofue 1977, 1994). Using morphology analysis, Liu et al. (2024) also proposed that the NPS/eROSITA bubble is distant and giant structures close to GC. Sofue (2017) measured the HI gas density in the inner Milky Way. They found that there is a HI hole around the GC and the hole has a crater-shaped wall that coincides with the Loop I/NPS. Such discovery supports the GC origin of Loop I/NPS. The GC hypothesis is also supported by the fact that the measured H α -to-1.4 GHz radio intensity ratio for the Loop I/NPS is two orders of magnitude smaller than the typical shell-type SNRs (Sofue et al. 2023). The North-South asymmetry is explained by the lower density of the medium in the southern hemisphere. Expansion in a low density medium results in weak shock acceleration efficiency, and weak radiation (Lallement 2023; Sarkar 2019).

In radio band, Loop I/NPS's emission is mainly the synchrotron radiation (Borka 2007). There have been many models developed to explain the Loop I/NPS's morphology. In the supernova remnants (SNRs) scenario, the bright ridge origins from compressed magnetic field and/or enhanced cosmic ray, i.e. the emissivity at the shell is larger than the interior. The asymmetry of the loop is due to the inhomogeneous distribution of the gas (see Dickinson 2018 and references therein). In ultralong wavelength band (wavelength $\gtrsim 10$ m or frequency $\lesssim 30$ MHz), particularly when frequency $\lesssim 10$ MHz, the free-free absorption by diffuse electrons in the interstellar medium (ISM) is important and may change the observed morphology of radio sky, including the Loop I/NPS structure (Cong et al. 2021, 2022). Loop I/NPS, at least the low Galactic latitude part, will be dark if it is located at the GC, but will be still bright if it is nearby SNRs. Cong et al. (2021) pointed out that

the ultralong wavelength observations have the potential to solve the problems of Loop I/NPS's origin. In this paper, we explicitly investigate this problem. We develop phenomenological models to predict the observational features of Loop I/NPS for the SNR model and GC model, at ultralong wavelength band. The outline of this paper is as follows: In Sec. 2, We present the emissivity model for the disk and Loop I/NPS structure. Then we develop an electron density model for Loop I/NPS. Main results are presented in Sec. 3 We summarize the results in Sec. 4 and discuss some uncertainties in Sec. 5.

2. METHODS

In this work, we model the Galactic emissivity as comprising of a smooth disk component—including both thin and thick disks (It is worth noting that this is not the same concept as the optical thin disk and thick disk; these thin and thick disks describe the diffuse components, primarily originating from synchrotron radiation.), and a Loop I/NPS structure. Model parameters are derived by reproducing the observed Haslam 408 MHz all-sky map (Remazeilles et al. 2015), and extrapolate to lower frequencies by power-law formula.

2.1. The disk emissivity

The disk emissivity is composed of a thin disk component and a thick disk component. It can be written as

$$\epsilon_{\text{disk}}(\nu|R,Z) = \sum_{i} A_{i} \exp\left\{-b(\alpha_{i}) \left[\left(\frac{R}{R_{i}}\right)^{\frac{1}{\alpha_{i}}} - 1 \right] \right\} \times \operatorname{sech}\left(\frac{Z}{Z_{i}}\right)^{\gamma_{i}} \left(\frac{\nu}{\nu_{*}}\right)^{\beta_{G}}, \tag{1}$$

where R and Z are cylindrical Galactic coordinates, ν is the frequency, and $i \in [\text{thin, thick}]$. The radial dependence form of Eq. (1) is actually the Sérsic profile (Sersic 1968) that is widely used to fit the surface brightness distribution of elliptical galaxies, as well as the disk and bulge components of other galaxy types. A_i denotes the emissivity at the effective radius R_i , which encompasses half of the total profile intensity in Z=0 plane. The index α_i indicates the profile's curvature in radial, and the $b(\alpha)$ is approximately as $2\alpha - \frac{1}{3} + \frac{4}{405\alpha} + \frac{46}{25515\alpha^2}$

The frequency-independent parameters A_i , R_i , α_i , Z_i , and γ_i are obtained by fitting the free-free and isotropic extragalactic radiation subtracted Haslam 408 MHz map. The isotropic extragalactic background and free-free emission are all the same to Cong et al. (2021). The parameter β_G is typically a function of frequency

and spatial position. However, here we consider a constant β_G as our fidutial model. Throughout this paper, we adopt $\beta_G = -2.51$ for the Galactic synchrotron radiation same as Cong et al. (2021).

2.2. The Loop I/NPS emissivity

We begin by modeling the Loop I/NPS emissivity as a sphere with a thin and dense spherical shell, which we then trim to reproduce the observed loop morphology. The sphere possesses a radius denoted as $r_{\rm L}$, with a shell of thickness $\Delta r_{\rm s}$. The emissivity of the shell is represented by $\epsilon_{\rm s}$, while the emissivity of the sphere's interior is indicated by $\epsilon_{\rm i}$. Specifically:

$$\epsilon_{L}(r) = \begin{cases} \epsilon_{i} & r < r_{L} - \Delta r_{s} \\ \epsilon_{s} & r_{L} - \Delta r_{s} \le r \le r_{L} \\ 0 & r > r_{L} \end{cases}$$
 (2)

where r is the distance to the center of the Loop I sphere. Given that $\epsilon_s \gg \epsilon_i$, the projection of the sphere onto the celestial sphere results in a limb-brightened loop.

In this study, we examine two potential scenarios for the origin of Loop I/NPS: the shell-like SNRs model, which attributes Loop I/NPS to supernova remnants near the Sun, and the Galactic Center (GC) model, which places Loop I/NPS closer to the center of the Galaxy, akin to the Fermi Bubble. For both models, the angular size of Loop I/NPS is approximately $\sim 116^\circ$ (Mertsch & Sarkar 2013), implying differences in its physical size.

2.2.1. The shell-like SNRs model

In this model, we adopt the direction (the latitude and longtitude) of Loop I/NPS center and its distance to Sun given in Berkhuijsen et al. (1971); Mertsch & Sarkar (2013). The observed morphology of Loop I/NPS exhibits irregular characteristics. This is likely a result of the interaction between the supernova remnant and a joint envelope formed by the stellar winds of the Sco-Cen OB association or the Local Hot Bubble. (Egger & Aschenbach 1995; Vidal et al. 2015). Thus, it is necessary to eliminate certain portions of the emissivity sphere to accurately reproduce the observed morphology.

We first remove the portion of Loop I/NPS below the Galactic plane, Z < 0, to address the north-south asymmetry. Then we create a suppositional 3D ellipse centered at Galactic coordinates (-8.522, -0.089, 0.029) kpc with axes of ($2r_{\rm L}, 0.4r_{\rm L}, 2r_{\rm L}$), and remove the volume in Loop I/NPS overlaps with this ellipse. This is motivated by the east-west asymmetry of the observed morphology. Following this processing, we successfully produce the morphological features of Loop I as observed in the Haslam 408 MHz map.

2.2.2. The Galactic Center model

In the GC model, Loop I/NPS is considered as the post-shock medium (Mou et al. 2023a). It consistently aligns with the shape of the Fermi Bubble and the X-ray Bubble (Mou et al. 2023b). Same to the shell-like SNRs model, here we also remove the portion where Z<0. However in the GC model, the Z<0 portion is a small fraction compared to its northern counterpart, because the center of Loop I/NPS is well above the Galactic plane. Then we create a suppositional sphere in 3D space centered at (-5.262, -5.608, 1.142) kpc with a radius of $r_{\rm L}$ and eliminate the overlap between Loop I/NPS and the sphere to address the east-west asymmetry.

Table 1. $R_{\rm L}, Z_{\rm L}$ and $\Phi_{\rm L}$ are Galactic cylinder coordinates of the Loop I/NPS center.

SNR	GC
8.3	1.5
0.07	5.0
-179.19	-90
0.22	7.8
0.02	2.5
147.5	4.67
1.53	0.0
	8.3 0.07 -179.19 0.22 0.02 147.5

The parameters of the two Loop I/NPS models are listed in Tab. 1. Finally, the total emissivity of the Galaxy is derived from the combined emissivities of the thin disk, the thick disk, and the Loop I/NPS,

$$\epsilon_{\text{MW}}(\nu|R,Z) = \epsilon_{\text{disk}}(\nu|R,Z) + \epsilon_{\text{L}}(\nu|R,Z).$$
 (3)

Fig. 1 shows the emissivity distribution slices of the Milky Way, encompassing both the disk and Loop I/NPS in the two models. We obtain the skymap by integrating this emissivity along each line-of-sight, and show the results at 408 MHz in Fig. 2. Our emissivity models replicate the morphology of the observed sky map very well.

2.3. The electron density of Loop I

NE2001 is a model for Galactic free electron distribution (Cordes & Lazio 2002, 2003). It comprises five components: the thin and thick disks, the spiral arms, the Galactic center, and the local interstellar medium (ISM), which includes known dense clumps and voids. In this model, Loop I/NPS is a hemisphere void above the Galactic plane, with a thin shell. We basically adopt the NE2001 model for Milky Way's electron distribution, however we improve the Loop I/NPS structure. We

assume that the geometry of Loop I/NPS is the same to the emissivity model, but derive the electron densities from HaloSat X-ray observations (LaRocca et al. 2020a).

HaloSat is a satellite designed to detect diffuse X-ray emissions in the range 0.4 - 7.0 keV (Kaaret et al. 2019; LaRocca et al. 2020b). It has a full response field of view of 10°, which makes it a useful tool for probing the thermal X-ray emission from the free electrons of Loop I/NPS. HaloSat provides 14 pointing directions for the Loop I/NPS region. In work of LaRocca et al. (2020a), they propose that Loop I/NPS consists of a two-phase plasma: a cool component with an energy value of 0.087 keV (temperature $\sim 1.01 \times 10^6$ K) and a hot component with an average energy of 0.274 keV (temperature \sim $3.18 \times 10^6 \text{ K})^1$. Both of them are optically thin and in ionization equilibrium. They fitted the EM values of the two components of Loop I/NPS for the 14 pointing directions according to observed X-ray spectral. The value of EM decrease with the increase in angle relative to the Galactic center. We sum the EM for the cool and hot components to obtain the full EM for Loop I/NPS. In principle, if the Loop I is an unknown structure at the Galactic center, the observed EM is from both the Loop I and the in-between ISM. However, since the emissivity of Loop I dominates over the in-between ISM and form the NPS, here we naively assume the EM is also mainly from Loop I.

For each i-th line-of-sight, the EM of Loop I/NPS is

$$EM_{i} = \sum_{i=1}^{N_{i}} \frac{1}{f_{e}} n_{e,j}^{2} \Delta s_{i,j},$$
 (4)

where this line-of-sight passes N_j segments in the Loop I/NPS. For the *j*-th segment, the electron density is $n_{e,j}$ and the path-length is $\Delta s_{i,j}$. f_e is a filling factor and we use $f_e = 0.5$ (LaRocca et al. 2020a).

We divide the spherical coordinates θ of the Loop I/NPS-centered frame sphere shell into 20 parts and ϕ coordinates into 4 parts. The interior of the sphere is a single part with uniform density. We then perform MCMC fitting for all the 14 line-of-sights in HaloSat observations, to find the electron density for each segment. For the segment without any line-of-sights passing, the electron density is assigned by interpolation from the nearest segment.

Fig. 3 shows the electron density distribution for the slices of X' = 0, Y' = 0 and Z' = 0 in Loop I cen-

 $^{^1}$ LaRocca et al. (2020a) suppose that Loop I/NPS fully contribute to the fitted hot component, and primarily contribute to the fitted cool component.

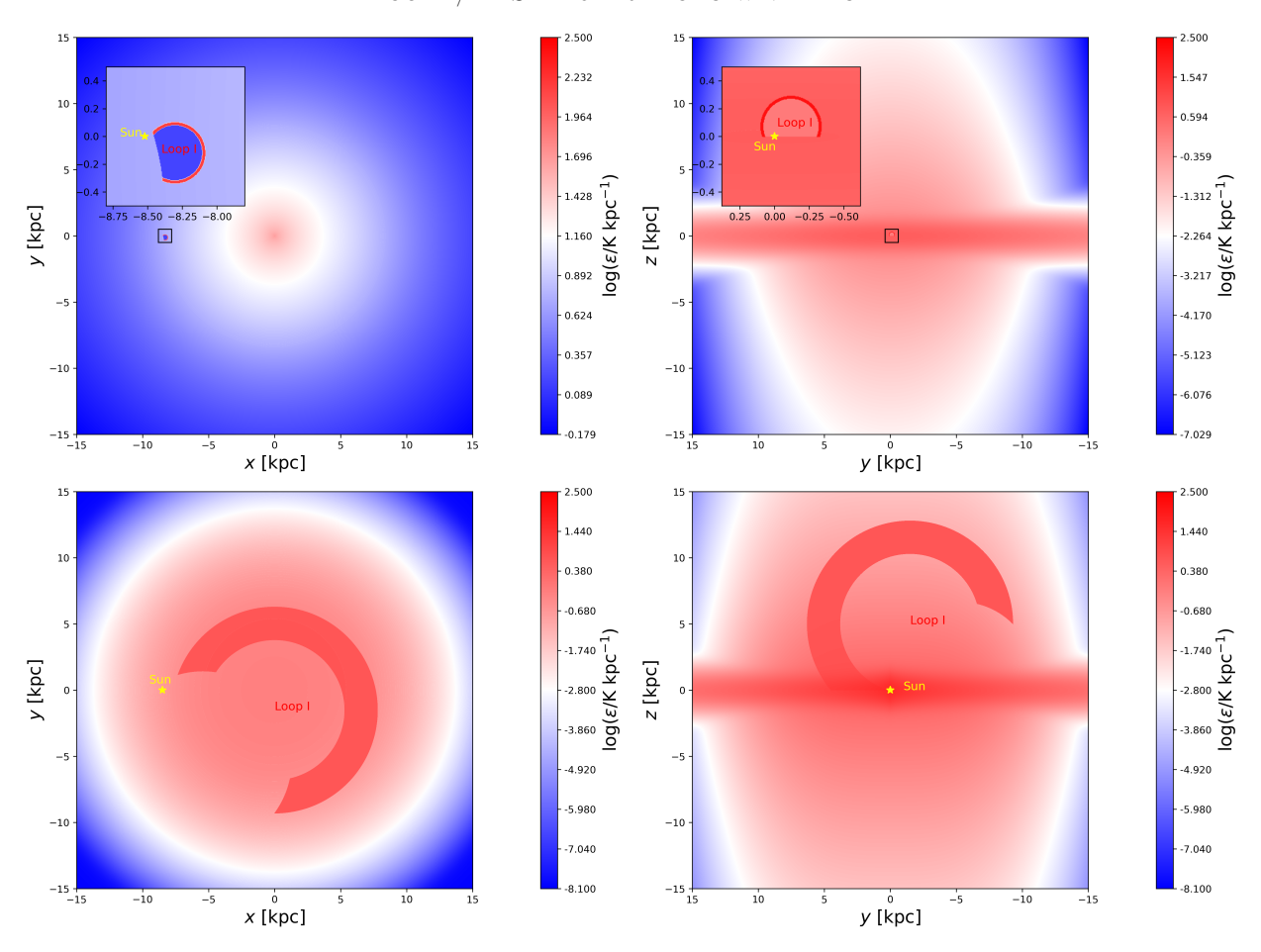


Figure 1. The emissivity distribution at the Loop I/NPS-centered X - Y (face on,left) and Y - Z (edge on, right) plane, at 408 MHz. **Top**: The shell-like SNRs model; **Bottom**: Galactic Center (GC) model.

tered coordinate frame. Fig. 4 illustrates the integrated free-free absorption optical depth of Loop I/NPS at 1 MHz(Condon & Ransom 2016),

$$\tau_{\nu} \approx 3.28 \times 10^{-7} \left(\frac{T_e}{10^4 \,\mathrm{K}}\right)^{-1.35} \left(\frac{\nu}{\mathrm{GHz}}\right)^{-2.1} \left(\frac{\mathrm{EM}}{\mathrm{pc} \,\mathrm{cm}^{-6}}\right),$$
(5)

assuming electron temperature $T_e = 10^6$ K, for the two models. Interestingly, the optical depth maps do not show loop-like feature, this is consistent with the EM map derived from Planck observations (Planck Collaboration et al. 2020).

We find that actually the optical depth from the Loop I/NPS itself is small, primarily because the electrons therein are hot. The EM derived from HaloSat observations is for electrons with temperature $\sim 10^6$ K, much hotter than the typical WIM (several thousands K) in the Milky Way. However, it seems that in Loop I/NPS electrons with temperature close to the typical WIM are few, because in the H α sky map there is no corresponding loop-like structure found (Haffner et al. 2003). We check that, if we replace the Loop I model with a hemi-

sphere with radius 7.8 kpc (0.22kpc), thickness of the shell 2.5 kpc (0.02kpc), density of the shell 0.01 cm⁻³ (0.081 cm⁻³) and density of the sphere interior 0.005 cm⁻³ (0.024 cm⁻³), and temperature 10^6 K. The optical depth is still always lower than $\sim 3 \times 10^{-3}$. If the tmeperature is set to be 8000 K, then the optical depth can reach up to ~ 2 , reducing the radiation behind Loop I/NPS by at most 14%. In short summary: the self-absorption of the Loop I/NPS emission should have modest effects on the final sky map.

3. RESULTS

With the modeled 3D emissivity and free electron distribution, the sky map is obtained by performing intergration of the rediative transfer function along each line of sight. Considering the free electron distribution within the Milky Way, radiation from Loop I/NPS would experience absorption in the ultra-long wavelength band. If Loop I/NPS is from nearby supernova remnant (SNR), the absorption between Loop I/NPS and observer would be minimal, whereas if it is located near the Galactic Centre, the influence of absorption by

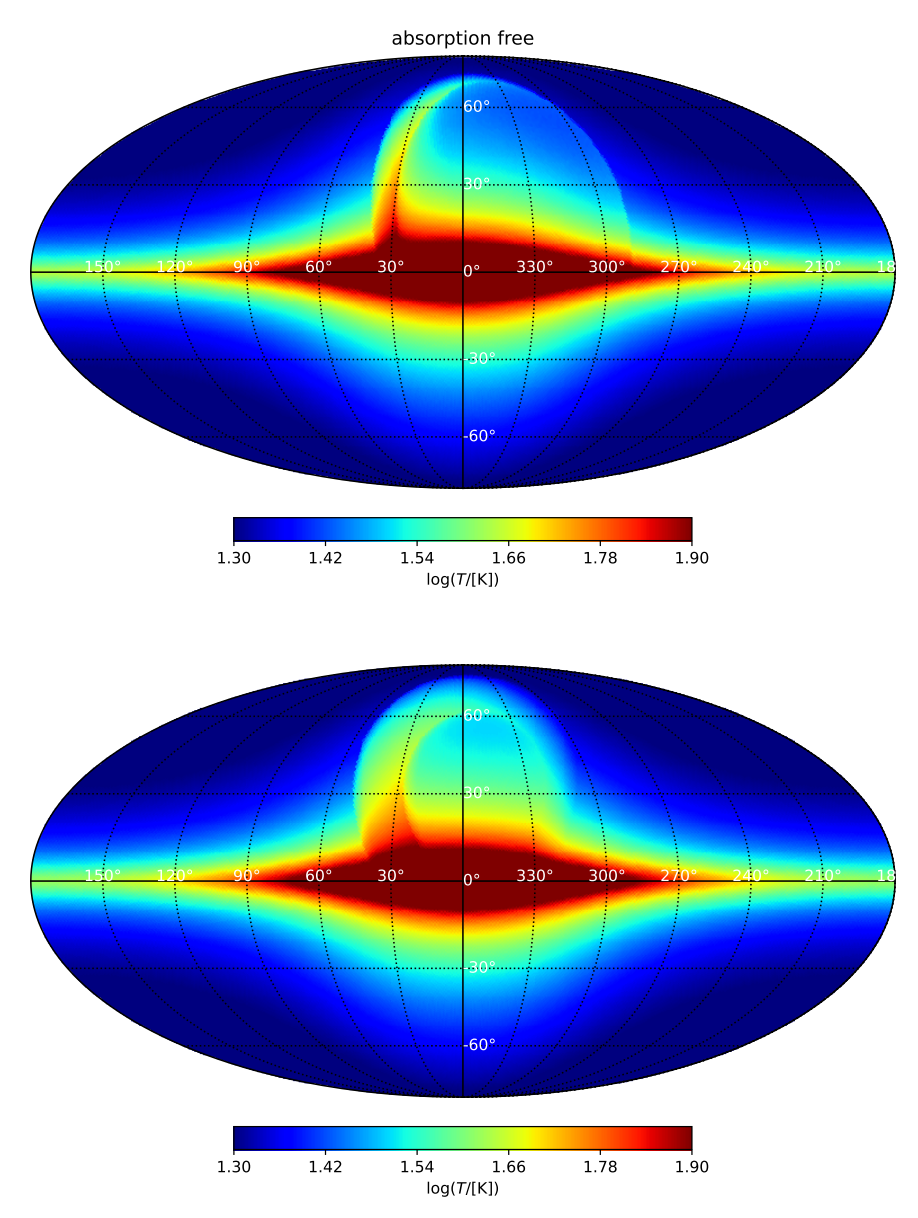


Figure 2. The sky map at 408 MHz for the shell-like SNRs (top) and the Galactic center (bottom) model respectively.

ISM would be significant. Our modelling and calculations validate these predictions. In Figs. 5 we present the predicted sky maps at frequencies 10, 3, and 1 MHz, respectively, for our two Loop I/NPS origin models. Clearly, at the frequency as low as 1 MHz, the high Galactic latitude regions are brighter while the Galactic disk is darker. However, on the Galactic disk, at the directions where the projection of electron density is low in the NE2001 model, say the LDR (low density region, $30^{\circ} \lesssim l \lesssim 90^{\circ}$) and the Local Hot Bubble (around $l \sim 60^{\circ}$), and LSB (local superbubble $l \sim 240^{\circ}$), there are bright patches. This is already pointed out in Cong et al. (2021).

However, in the shell-like SNRs model the full Loop I/NPS is still a bright structure. This is because it is very close to the observer, the absorption by the ISM electrons is negligible. However, in the GC model, the morphology is quite different. The Loop I/NPS disappears at $b \lesssim 30^\circ$, due to the absorption of electrons between the GC and the observer. So indeed, the ultralong wavelength observations have the ability to distinguish the models for Loop I/NPS's origin. We also note that, in both SNRs model and GC model, at $b \gtrsim 30^\circ$, the Loop I/NPS is always a bright structure. It means that the absorption toward the high Galactic latitudes, even until the GC, is still weak at least until 1 MHz. This

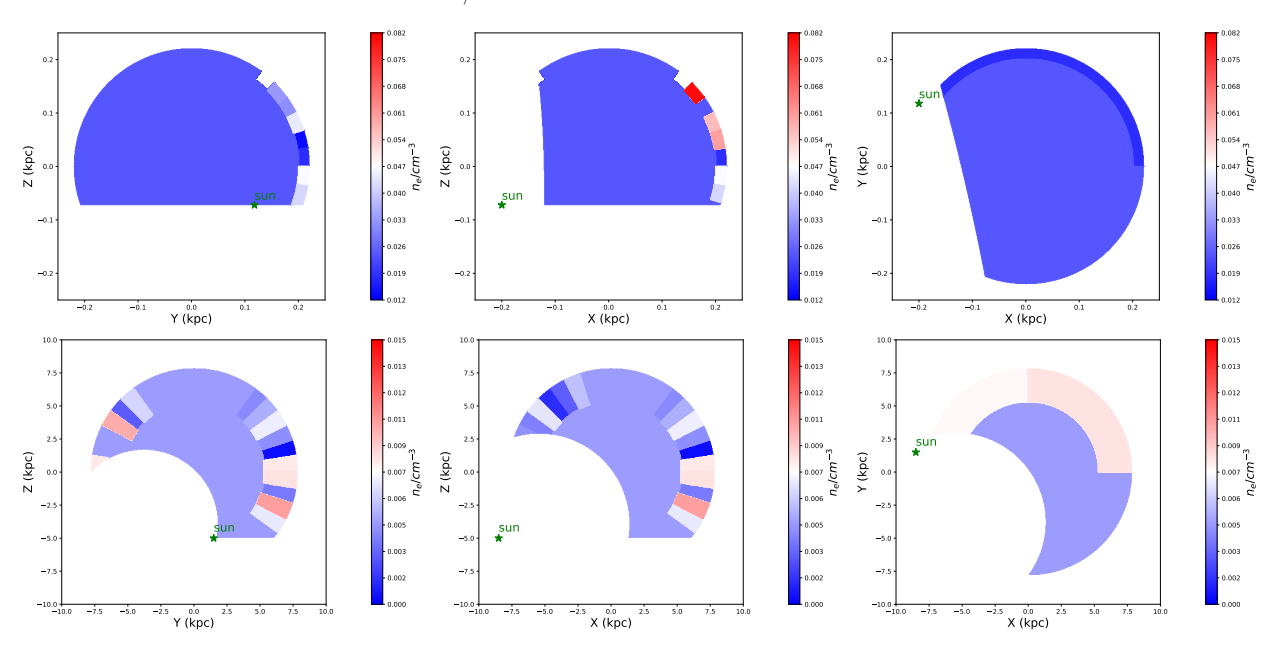


Figure 3. The Loop I/NPS electron density constructed from HaloSat observations for the shell-like SNRs (top) and GC model (bottom) respectively. From left to right, we plot the X' = 0, Y' = 0 and Z' = 0 planes respectively, in the Loop I/NPS centered coordinate frame, and mark the Sun's position of the projection in each panel. In the top panels the Sun's position is (-0.196, 0.118, -0.072) kpc, while in the bottom panels it is (-8.5, 1.5, -5) kpc.

is further helpful for deriving the electron distribution along the Galactic height.

4. SUMMARY

In this paper, we investigated the Loop I/NPS structure feature at ultralong wavelength band. We considered two models: in the shell-like SNRs model, the Loop I/NPS is a SNR close to our Sun; in the GC model it is located close to the center of our Galaxy and it has large physical size. All these two models can reproduce the observational feature (the loop-like) at high frequencies where the free-free absorption is negligible. However, at ultralong wavelength band where the free-free absorption is efficient ($\nu \lesssim 3$ MHz), the loop-like feature differs significantly in the two models. In the shell-like SNRs model, the Loop I/NPS is still bright at frequency even as low as 1 MHz. However, in the GC model, due to the free-free absorption by the ISM between the GC and the Sun, the Loop I/NPS structure becomes dark or even fully disappears at $b \lesssim 30^{\circ}$. However, at high Galactic latitudes, $b \gtrsim 30^{\circ}$, the Loop I/NPS structure is still a notable feture in the sky. As a reference, we note that both the Faraday rotation depolarization amount and Faraday depth are heavily distinguishable above and below $b \sim 30-40^{\circ}$ (Sun et al. 2015; Dickinson 2018). The upcoming ultralong wavelength observations, for example the DSL, FARSIDE, et al. (Burns & Hallinan 2020; Chen et al. 2021, 2024), have the potential to distinguish these two models.

We added such structure to the version 2.0 of our sky model ULSA-v2.

5. DISCUSSION

We did not employ any physical hypothesis on the origin of Loop I/NPS, which is still in debate. just adopted phenomenological models to describe its location, size and emissivity. Our forecast on the Loop I/NPS morphology in ultralong wavelength band should be robust. However, we note that at different wavelengths Loop I/NPS morphology is different. At radio band, it is an arc above the Galactic plane, however at soft X-ray band it extends to below the Galactic plane and forms dual bubbles (Predehl et al. 2020). In the polarization map, there are many spurs inside the Loop I/NPS (above and below the Galactic plane) and they are all rooted on Galactic plane (Bennett et al. 2013; Planck Collaboration et al. 2016; Dickinson 2018). Since our phenomenological model only aims to reproduce the observed Loop I/NPS morphology at the 408 MHz, so it is possible that in ultra-long wavelength band, there are new structures near the Loop I/NPS. They may confuse our identification of the Loop I/NPS origin.

Regarding the Loop I/NPS, there are arguments supporting both a local feature and a GC feature. It is also possible that a local feature coincides with the GC feature. If Loop I/NPS comprises two visually overlapping components, three hypotheses can be considered in this context. The first suggests that the high-latitude portion of Loop I/NPS is located at the Galactic Centre,

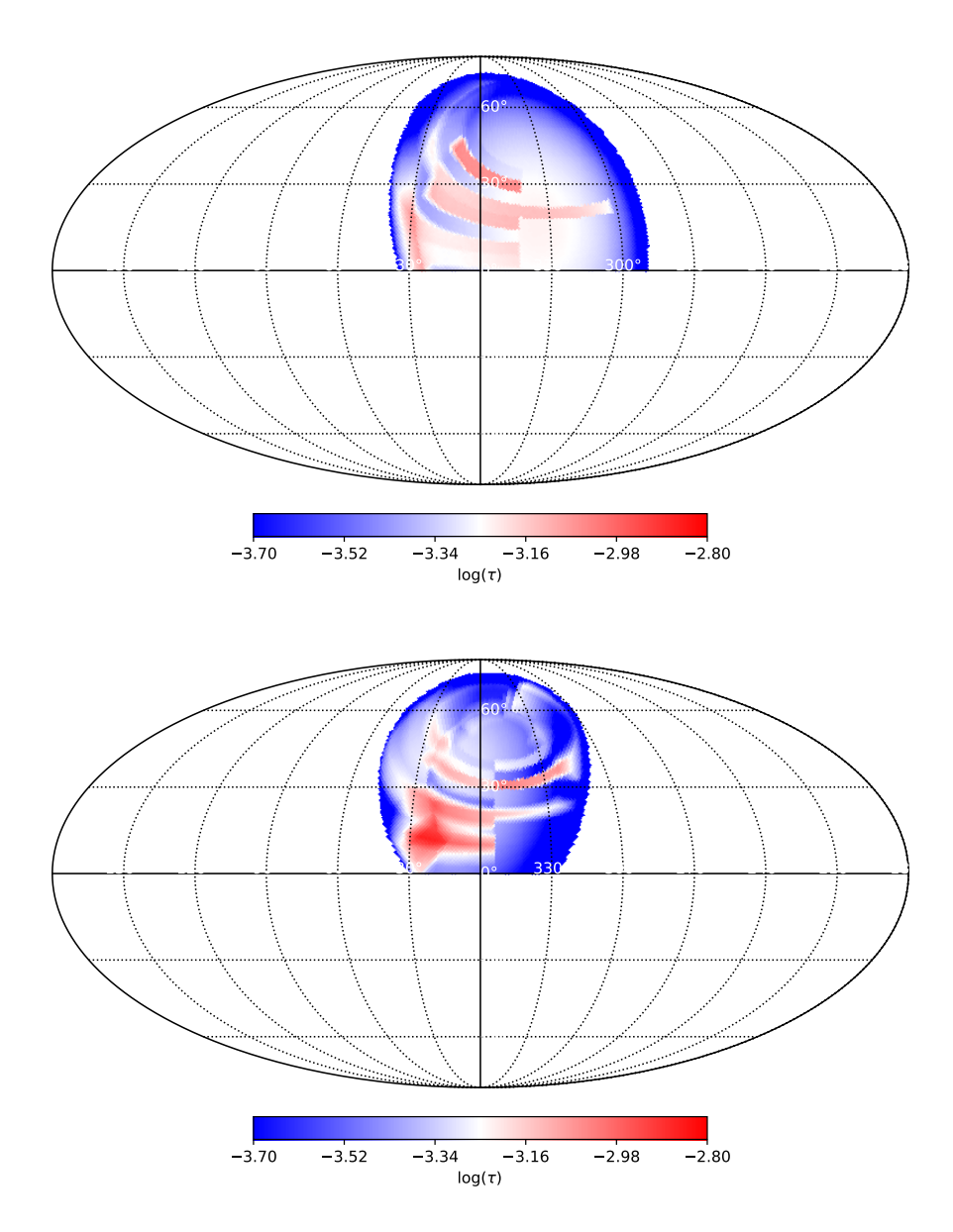


Figure 4. The free-free absorption optical depth of Loop I/NPS at 1 MHz for the shell-like SNRs model (top) and GC model (bottom). The vertical line is a virtual effect resulting from the division into four parts along the Φ direction, with each part exhibiting slight variations in value.

while the remaining segment originates from a nearby source. Due to weaker absorption at high galactic latitudes, Loop I/NPS would still manifest as a bright, complete arc in the ultralong wavelength band, rendering it indistinguishable from the shell-like SNRs model. The second hypothesis proposes that the high-latitude portion is a nearby structure, while the remaining segment resides at the Galactic Centre. Due to stronger absorption at low galactic latitudes, only the high-latitude regions would be visible in the ultralong wavelength band, making it indistinguishable from the GC model. The final hypothesis involves an overlap of nearby and Galac-

tic Centre components throughout Loop I/NPS. If the entire loop is observable at ultra-long wavelengths, the high-latitude section would consist of both nearby and Galactic Centre components, while the lower latitude region would predominantly originate from nearby emission. This scenario may still remain indistinguishable from the shell-like SNR model.

This scenario can be assessed by analysing high-frequency polarization in the absence of absorption effects. If Loop I/NPS is composed of two physically unrelated and spatially distinct components, the probability of observing a coherent polarization structure is signifi-

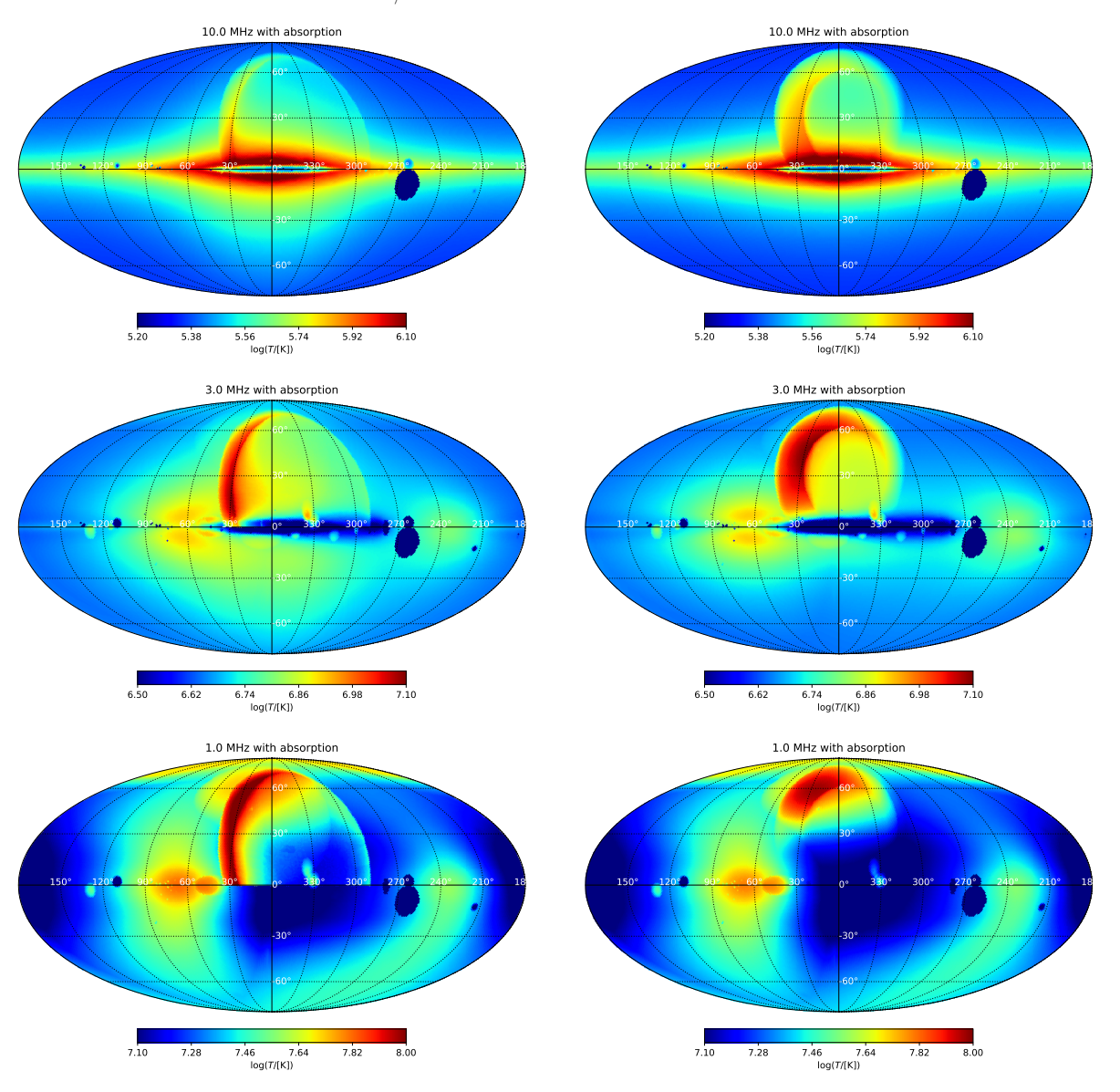


Figure 5. The predicted sky maps at frequencies 10, 3 and 1 MHz respectively, for the shell-like SNRs model of Loop I/NPS(left column) and GC model(right column).

cantly reduced. For instance, while the WMAP/Planck polarization maps suggest a unified structure for Loop I/NPS (Planck Collaboration et al. 2016; Dickinson 2018), this feature is not apparent in the 1.4 GHz polarization map (Reich & Reich 2009), possibly due to depolarization effects near the Galactic plane.

In our paper, the spectrum indices of $\epsilon_{\rm disk}$ and $\epsilon_{\rm L}$ are the same. Therefore the change of morphology additional to the simple extrapolation from power-law spectrum is purely attributed to the free-free absorption. However, if the Loop I/NPS spectrum indices dependent

dence on Galactic latitudes is different from other regions, i.e. sharper at high Galactic latitudes and shallower at low Galactic latitudes, it may also result in morphology analogous to free-fee absorption. However, we check that, at least until ~ 20 MHz, there is no such phenomena, see also Guzmán et al. (2011).

ACKNOWLEDGMENTS

This work was supported by National Key R&D Program of China No. 2022YFF0504300; National Natural Science Foundation of China (NSFC) grants 12361141814.

REFERENCES

- Baldwin, J. E. 1955, MNRAS, 115, 684, doi: 10.1093/mnras/115.6.684
- Bennett, C. L., Larson, D., Weiland, J. L., et al. 2013, ApJS, 208, 20, doi: 10.1088/0067-0049/208/2/20
- Berkhuijsen, E. M., Haslam, C. G. T., & Salter, C. J. 1971, A&A, 14, 252
- Borka, V. 2007, MNRAS, 376, 634, doi: 10.1111/j.1365-2966.2007.11499.x
- Breitschwerdt, D., & de Avillez, M. A. 2006, A&A, 452, L1, doi: 10.1051/0004-6361:20064989
- Burke, B. F., Graham, & Wilkinson, P. N. 2019, An introduction to radio astronomy, 4th edition (Cambridge University Press)
- Burns, J. O., & Hallinan, G. 2020, in American Astronomical Society Meeting Abstracts, Vol. 235, American Astronomical Society Meeting Abstracts #235, 130.01
- Centurion, M., & Vladilo, G. 1991, ApJ, 372, 494, doi: 10.1086/169995
- Chen, X., Yan, J., Deng, L., et al. 2021, Philosophical Transactions of the Royal Society of London Series A, 379, 20190566, doi: 10.1098/rsta.2019.0566
- Chen, X., Gao, F., Wu, F., et al. 2024, arXiv e-prints, arXiv:2403.16409, doi: 10.48550/arXiv.2403.16409
- Condon, J. J., & Ransom, S. M. 2016, Essential Radio Astronomy
- Cong, Y., Yue, B., Xu, Y., et al. 2021, ApJ, 914, 128, doi: 10.3847/1538-4357/abf55c
- Cong, Y., Yue, B., Xu, Y., Shi, Y., & Chen, X. 2022, ApJ, 940, 180, doi: 10.3847/1538-4357/ac9df7
- Cordes, J. M., & Lazio, T. J. W. 2002, arXiv e-prints, astro. https://arxiv.org/abs/astro-ph/0207156
- —. 2003, arXiv e-prints, astro. https://arxiv.org/abs/astro-ph/0301598
- Cox, D. P., & Reynolds, R. J. 1987, ARA&A, 25, 303, doi: 10.1146/annurev.aa.25.090187.001511
- de Geus, E. J. 1992, A&A, 262, 258
- Dickinson, C. 2018, Galaxies, 6, 56, doi: 10.3390/galaxies6020056
- Dowell, J., Taylor, G. B., Schinzel, F. K., Kassim, N. E., & Stovall, K. 2017, MNRAS, 469, 4537, doi: 10.1093/mnras/stx1136
- Eastwood, M. W., Anderson, M. M., Monroe, R. M., et al. 2018, AJ, 156, 32, doi: 10.3847/1538-3881/aac721
- Egger, R. J., & Aschenbach, B. 1995, A&A, 294, L25, doi: 10.48550/arXiv.astro-ph/9412086
- Guzmán, A. E., May, J., Alvarez, H., & Maeda, K. 2011, A&A, 525, A138, doi: 10.1051/0004-6361/200913628

- Haffner, L. M., Reynolds, R. J., Tufte, S. L., et al. 2003, ApJS, 149, 405, doi: 10.1086/378850
- Hanbury Brown, R., Davies, R. D., & Hazard, C. 1960, The Observatory, 80, 191
- Haslam, C. G. T., Salter, C. J., Stoffel, H., & Wilson, W. E. 1982, A&AS, 47, 1
- Intema, H. T., Jagannathan, P., Mooley, K. P., & Frail,
 D. A. 2017, A&A, 598, A78,
 doi: 10.1051/0004-6361/201628536
- Iwan, D. 1980, ApJ, 239, 316, doi: 10.1086/158113
- Iwashita, R., Kataoka, J., & Sofue, Y. 2023, ApJ, 958, 83, doi: 10.3847/1538-4357/ad0374
- Kaaret, P., Zajczyk, A., LaRocca, D. M., et al. 2019, ApJ, 884, 162, doi: 10.3847/1538-4357/ab4193
- Kataoka, J., Sofue, Y., Inoue, Y., et al. 2018, Galaxies, 6, 27, doi: 10.3390/galaxies6010027
- Lallement, R. 2023, Comptes Rendus Physique, 23, 1, doi: 10.5802/crphys.97
- Lallement, R., Capitanio, L., Ruiz-Dern, L., et al. 2018, A&A, 616, A132, doi: 10.1051/0004-6361/201832832
- Landecker, T. L., & Wielebinski, R. 1970, Australian Journal of Physics Astrophysical Supplement, 16, 1
- Large, M. I., Quigley, M. F. S., & Haslam, C. G. T. 1966, MNRAS, 131, 335, doi: 10.1093/mnras/131.3.335
- Large, M. I., Quigley, M. J. S., & Haslam, C. G. T. 1962, MNRAS, 124, 405, doi: 10.1093/mnras/124.5.405
- LaRocca, D. M., Kaaret, P., Kuntz, K. D., et al. 2020a, ApJ, 904, 54, doi: 10.3847/1538-4357/abbdfd
- LaRocca, D. M., Kaaret, P., Kirchner, D. L., et al. 2020b, Journal of Astronomical Telescopes, Instruments, and Systems, 6, 014003, doi: 10.1117/1.JATIS.6.1.014003
- Liu, T., Merloni, A., Sanders, J., et al. 2024, ApJL, 967, L27, doi: 10.3847/2041-8213/ad47e0
- Mertsch, P., & Sarkar, S. 2013, JCAP, 2013, 041, doi: 10.1088/1475-7516/2013/06/041
- Mou, G., Wu, J., & Sofue, Y. 2023a, A&A, 676, L3, doi: 10.1051/0004-6361/202245401
- Mou, G., Sun, D., Fang, T., et al. 2023b, Nature Communications, 14, 781, doi: 10.1038/s41467-023-36478-0
- Panopoulou, G. V., Dickinson, C., Readhead, A. C. S., Pearson, T. J., & Peel, M. W. 2021, ApJ, 922, 210, doi: 10.3847/1538-4357/ac273f
- Patra, N., Subrahmanyan, R., Sethi, S., Udaya Shankar, N., & Raghunathan, A. 2015, ApJ, 801, 138, doi: 10.1088/0004-637X/801/2/138
- Planck Collaboration, Ade, P. A. R., Aghanim, N., et al. 2016, A&A, 594, A25, doi: 10.1051/0004-6361/201526803

- Planck Collaboration, Aghanim, N., Akrami, Y., et al. 2020, A&A, 641, A1, doi: 10.1051/0004-6361/201833880
- Predehl, P., Sunyaev, R. A., Becker, W., et al. 2020, Nature, 588, 227, doi: 10.1038/s41586-020-2979-0
- Quigley, M. J. S., & Haslam, C. G. T. 1965, Nature, 208, 741. https://api.semanticscholar.org/CorpusID:4205652
- Reich, P., & Reich, W. 1986, A&AS, 63, 205
- Reich, W., & Reich, P. 2009, in IAU Symposium, Vol. 259, Cosmic Magnetic Fields: From Planets, to Stars and Galaxies, ed. K. G. Strassmeier, A. G. Kosovichev, & J. E. Beckman, 603–612,
 - doi: 10.1017/S1743921309031433
- Reis, W., & Corradi, W. J. B. 2008, A&A, 486, 471, doi: 10.1051/0004-6361:20077946
- Remazeilles, M., Dickinson, C., Banday, A. J., Bigot-Sazy, M. A., & Ghosh, T. 2015, MNRAS, 451, 4311, doi: 10.1093/mnras/stv1274
- Roger, R. S., Costain, C. H., Landecker, T. L., & Swerdlyk, C. M. 1999, A&AS, 137, 7, doi: 10.1051/aas:1999239
- Sallmen, S. M., Korpela, E. J., & Yamashita, H. 2008, ApJ, 681, 1310, doi: 10.1086/588802

- Santos, F. P., Corradi, W., & Reis, W. 2011, ApJ, 728, 104, doi: 10.1088/0004-637X/728/2/104
- Sarkar, K. C. 2019, MNRAS, 482, 4813, doi: 10.1093/mnras/sty2944
- Sersic, J. L. 1968, Atlas de Galaxias Australes
- Shchekinov, Y. 2018, Galaxies, 6, 62, doi: 10.3390/galaxies6020062
- Sofue, Y. 1977, A&A, 60, 327
- —. 1994, ApJL, 431, L91, doi: 10.1086/187480
- —. 2000, ApJ, 540, 224, doi: 10.1086/309297
- —. 2015, MNRAS, 447, 3824, doi: 10.1093/mnras/stu2661
- —. 2017, PASJ, 69, L8, doi: 10.1093/pasj/psx067
- Sofue, Y., Habe, A., Kataoka, J., et al. 2016, MNRAS, 459, 108, doi: 10.1093/mnras/stw623
- Sofue, Y., Hamajima, K., & Fujimoto, M. 1974, PASJ, 26, 399
- Sofue, Y., Kataoka, J., & Iwashita, R. 2023, MNRAS, 524, 4212, doi: 10.1093/mnras/stad1985
- Su, M., Slatyer, T. R., & Finkbeiner, D. P. 2010, ApJ, 724, 1044, doi: 10.1088/0004-637X/724/2/1044
- Sun, X. H., Landecker, T. L., Gaensler, B. M., et al. 2015, ApJ, 811, 40, doi: 10.1088/0004-637X/811/1/40
- Vidal, M., Dickinson, C., Davies, R. D., & Leahy, J. P. 2015, MNRAS, 452, 656, doi: 10.1093/mnras/stv1328